



Investigation of angular aspects of a novel four-sector rotary dehumidifier configuration for HVAC applications

Ashutosh Kumar Verma ^{*}, Laxmikant Yadav

Department of Mechanical Engineering, NIT, Hamirpur, H.P., India



ARTICLE INFO

Keywords:

Novel configuration
Four-sector rotary dehumidifier
Two-dimensional mathematical model
Optimum angle

ABSTRACT

In buildings and industries, different humidity and temperature ranges may be required to fulfill the requirement. Desiccant-based air conditioning is more widely used to control the latent load using solar or waste heat efficiently. This work divides a rotary solid desiccant wheel into four sections: two process sections and two regeneration sections. Air from one process section (P1) is used in a cooling application with the aid of a cooling unit, while air from the other process section (P2) is used for warm and dry air applications. Furthermore, the input conditions and positioning of the regeneration sections (R1 and R2) are such that there is less carryover heat to the P1 section and more carryover heat to the P2 section, which is advantageous for both applications. The major objective of the present work is to investigate the optimal angular divisions of these four sections using a two-dimensional mathematical model. The developed mathematical model results are reported in good agreement with the experimental results of the literature. The optimal rotational speed of the wheel is computed as 15 revolutions per hour, and the optimal regeneration angles for R2 and R1 of the desiccant wheels are 100–110° and 115–125°, respectively.

Nomenclature

Symbol Description Units

A_{tc}	Total cross-sectional area of the channel	m^2
A_{cf}	Cross-sectional area of a flow channel	m^2
A_{dl}	Cross-sectional area of a desiccant layer	m^2
a	Aspect ratio	Dimensionless
c	Specific heat	$J \cdot kg^{-1} K^{-1}$
c_p	Specific heat at constant pressure	$J \cdot kg^{-1} K^{-1}$
D_{hf}	Hydraulic diameter	m
D_s	Surface diffusivity	$m^2 \cdot s^{-1}$
D_o	Ordinary diffusivity	$m^2 \cdot s^{-1}$
D_k	Knudsen diffusivity	$m^2 \cdot s^{-1}$
D_{ko}	Combined Knudsen and ordinary diffusivity	$m^2 \cdot s^{-1}$

* Corresponding author.

E-mail addresses: ashutosh@nith.ac.in, ashutosh.verma742@gmail.com (A.K. Verma).

D_{ma}	Mass diffusion coefficient of vapour in the air $m^2.s^{-1}$
h_{hc}	Heat transfer coefficient $W.m^{-2}.K^{-1}$
h_{mc}	Mass transfer coefficient $kg.m^{-2}s^{-1}$
q_{ad}	Heat of adsorption $J.kg^{-1}$
h_{fg}	Enthalpy of vaporization of water $J.kg^{-1}$
k	Thermal conductivity $W.m^{-1}.K^{-1}$
L_w	Wheel length m
M	Molecular weight g. mol ⁻¹
N	Rotational speed of the desiccant wheel rph
Nu_{FD}	Nusselt number of fully developed flow Dimensionless
Sh	Sherwood number Dimensionless
P_{fc}	Perimeter of a flow channel m
p_a	Atmospheric pressure Pa
p_v	Partial pressure of water vapour Pa
p_{vs}	Saturation vapour pressure Pa
r	Pore radius m
R	Separation factor Dimensionless
RH	Relative humidity %
T	Temperature K
t	Time s
u	Velocity of air $m.s^{-1}$
x	Direction of flow
y	Direction along the thickness of desiccant layer

Greek Symbol Description Units

2α	Channel height m
2β	Channel pitch m
$\delta_d/2$	Thickness of the desiccant layer m
ϵ	Porosity Dimensionless
Φ	Volume ratio of desiccant Dimensionless
ω	Humidity ratio $kg.kg^{-1}$
W	Water absorbed by the desiccant kg/kg of adsorbent
ρ	Density $kg.m^{-3}$
τ_g	Tortuosity factor Dimensionless
θ	Sector angle Degree

Subscript Description

a	Air
d	Desiccant
da	Dry air
dl	Desiccant layer
m	Matrix
R or r	Regeneration
P or p	Process
in	Inlet
v	Vapour
lw	Liquid water
out	Outlet

Abbreviations Description

RMRE	Relative moisture removal efficiency
rph	Revolution per hour
DCOP	Dehumidification coefficient of performance
CV	Control volume

1. Introduction

A rotary dehumidifier is a wheel that exchanges heat and mass and is commonly used to reduce humidity to an extremely low level. It is commercially used worldwide in the food and pharmaceutical industries, lithium battery manufacturing, cold stores, Data centers,

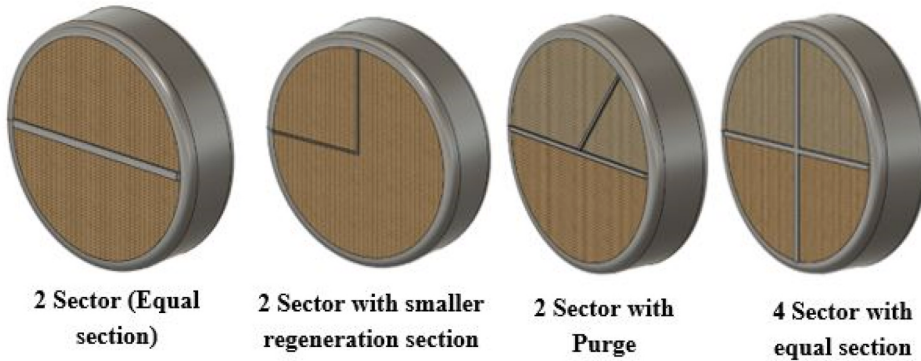


Fig. 1. Sector division of available desiccant wheel.

plastics processing, process industries, preservation and protection of equipment, materials, documents, etc. [1–5]. In hospitals, controlling humidity can help to improve indoor air quality and reduce the spread of airborne infections with more fresh air passing through the desiccant wheel [6]. Many researchers [7–10] have also used the rotary dehumidifier in air conditioning applications to control the latent load separately. They integrated desiccant wheels with evaporative cooling or vapour compression systems, ensuring the effective utilization of solar heat or waste heat. These hybrid systems improve overall performance and reduce harmful emissions into the environment. Numerous studies have already been carried out to enhance the rotary dehumidifier's moisture removal efficiency and energy performance. Recently, Elhady et al. [11] summarized the research on solid desiccant dehumidification systems and presented a critical review of configurations, techniques, and current trends. The development of the desiccant wheel from two sectors to four sectors is presented in Fig. 1. In a similar way, this study is based on novel rotary dehumidifier configurations. Hence, research related to different configurations and designs of the wheel is presented as literature in the subsequent paragraphs.

The novel configuration of rotary dehumidifier was initiated by Nagaya et al. [12] in 2006. They divided the silica gel desiccant wheel into three sections, namely, the process section (the first section having the largest area), the reactivation section (second section), and the heat collection section (third section) to neutralize the heat of adsorption and regeneration heat from the fresh air. Their results showed that three sections desiccant wheel provides faster drying than conventional desiccant drying. This research was extended by Golubovic et al. [13] in the year 2007. They renamed the heat collection (third) section as a purge section and evaluated the dehumidification and energy performance of rotary dehumidifiers with and without a heated purge. They investigated the purge angle (effective angle) of the wheel. They reported that the wheel with a heated purge angle provides lower moisture content and process air temperature than the wheel having no purge section. In addition to the heated purge, Yadav and Bajpai introduced a cooled purge which made four sector dehumidifiers [14]. They built a 1D numerical model, compared the performance of four-sector and two-sector desiccant wheels, and observed that the dehumidification efficiency of the two-sector wheel was exactly equal to the four-sector at twice the speed of four sector wheel. To enhance the regeneration performance of the desiccant wheel, Yadav [15] directed the output of the purge stream toward the regeneration section to utilize dehumidified air from purge to proper regeneration.

Similarly, to study the effect of purge angle and wheel rotation direction, Yadav and Yadav [16] mathematically investigated the performance of rotary dehumidifiers under different working conditions. Further, Mandegari et al. [17] introduced the concept of a novel purge section to enhance the dehumidification coefficient of performance (DCOP) of the desiccant wheel without any significant increase in wheel size. Motaghian and Pasdarshahri [18] also discussed the commercial use of the purge sector in the desiccant wheel and obtained a 30% improvement in COP and a 22% reduction in regeneration energy.

The research on novel configurations was further extended by Yadav and Yadav [19–20] to analyze the performance of desiccant wheels with an effective regeneration sector, ordinary regeneration sector, and effective adsorption sector for different working conditions. In continuation, Yadav and Yadav [21] introduced a third small sector in a conventional desiccant wheel and investigated the position of this third small section for better performance. Similarly, work on four to six-sector desiccant wheels [22–23] and two-stage dehumidification with a single rotary dehumidifier [24] was studied recently under different input conditions.

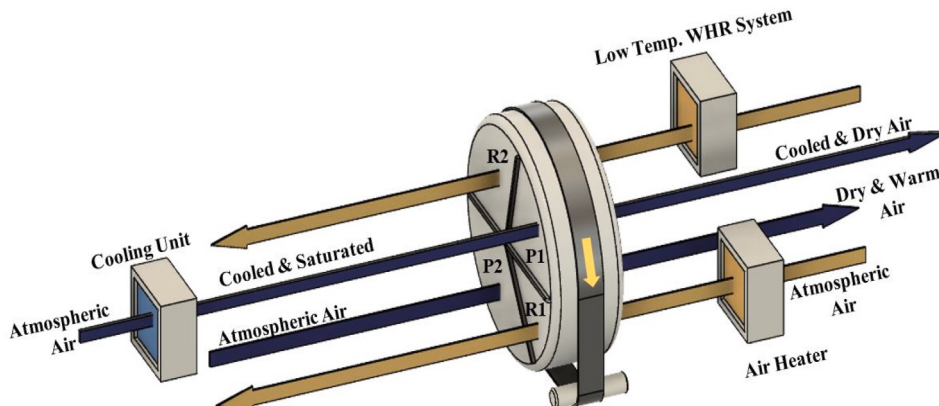
For air conditioning applications out of the total load, the desiccant wheel can effectively control the latent load to a very low humidity level. But it does not provide any cooling. Contrarily, it heats the air by heat of adsorption and carryover heat. This warm air increases the sensible cooling load of the cooling unit, which is not desirable [25]. To solve this problem, many researchers introduced the concept of a new design of rotary dehumidifier, which is an internally cooled desiccant wheel [26–29], and they found improvement in the efficiency of the wheel, but the major drawback is that size and cost of the internally cooled wheel is higher than the conventional desiccant wheel. Some more investigation [30–31] is based on the desiccant wheel's balanced and unbalanced flow. When the velocity of process air and regeneration air is the same, flow is known as balanced flow, and when velocities are different, it is known as unbalanced flow.

In 2010, Jeong et al. [32] analyzed the performance of four sector dehumidifiers and achieved air conditioning with the integration of VCRS. But here, the process section was in a series arrangement to obtain the two-stage dehumidification from the single wheel, and the purpose was only air conditioning. However, separate desiccant wheel sections for simultaneous cooling and drying with heating, such as combined heat and power (Cogeneration), have not been studied. As in a conventional desiccant wheel, only one section

Table 1

Sample of Design parameters by ASHRAE standard 170 [33].

Function of space	Pressure relationship to the adjacent area	Minimum outdoor air changes per hour	Minimum outdoor air changes per hour	Design Relative humidity, %	Design temperature, °C
Operating room	Positive	4	20	20–60	20 to 24
Emergency department public waiting area	Negative	2	12	Max 65	21 to 24
All room	Negative	2	12	Max 60	21 to 24
Patient room	No requirement	2	4	Max 60	21 to 24

**Fig. 2.** Schematic diagram of a novel configuration of the desiccant wheel.

produces one output, i.e., dry air. Then this dry air stream is divided into two streams, one for drying use and another stream towards the cooling section for air conditioning use. Further, in conventional dehumidifiers, the moisture removal and temperature rise of the process section are proportional [25]. Hence, independent control of moisture removal and temperature rise is complicated in conventional desiccant wheels.

There are many locations, ranging from the industrial sector to hospital buildings, where distinct air requirements are required, as presented in Table 1 [33]. More fresh air and less recirculation air have been needed in places like hospitals. When the outside room humidity is high, then fresh air requirements are costlier with conventional air conditioning systems. In such cases, a four-sector dehumidifier wheel-based air conditioning system may be useful for satisfying the two distinct needs of the buildings.

In addition, the innovation of four-sector dehumidifiers is the ability to maintain different regeneration temperatures in R1 and R2. As in this study, the regeneration temperature for R2 is 45 °C (lower temperature), and for R1, it is 60 °C (higher temperature). But a two-sector desiccant wheel can't do this because it only has one regeneration section. To address these issues with two-sector wheels, a novel configuration of four-sector desiccant wheels with two process sections, one for warm and dry air and the other for cool and dry air, has been proposed. The exit conditions of the four sectors' rotary dehumidifiers rely on the angular division of the wheel, making it essential to determine the ideal angle for the proposed novel rotary dehumidifier wheel. A comprehensive overview of the suggested system will be presented in the following section.

2. Layout and description of a four-sector desiccant wheel

The schematic diagram of the proposed system is shown in Fig. 2, where a desiccant wheel is rotating in a clockwise direction. The wheel is split into four sections, namely, process section 1(P1), regeneration section (R1), process section 2 (P2), and regeneration section 2 (R2), as shown in Fig. 2. Finding the optimal angle of these sections is the main objective of this study.

The four air streams pass through the four sections P1, R1, P2, and R2 of the rotary dehumidifier, as shown in Fig. 2. First, atmospheric air passes through the cooling unit, where it is cooled and saturated, and then it is sent to P1 for dehumidification. So, the resulting stream cools down and is dehumidified, which can be directly sent to condition space. In R1, a slightly higher temperature of the air has been used for regeneration so that we can utilize that heat in the P2 section for warm and dry air. In other words, the position of R1 in between P1 and P2 also justifies the wheel's rotation direction. As the wheel rotates from R1 to P2, the carryover heat may raise the temperature of P2. This higher temperature of P2 will be advantageous because P2 is reserved for warm and dry air. But the lower regeneration temperature of the air has been used in R2 because as the wheel rotates from R2 to P1, carryover heat releases into P1, and that may increase the temperature of the P2 stream, which is not desirable for cooling as P1 is reserved for cooling only.

Making a different angular division of the desiccant wheel for the proposed system is practically difficult. Hence, in this study 2D-mathematical transient model has been established to study the performance of the proposed system, which is presented in the next section.

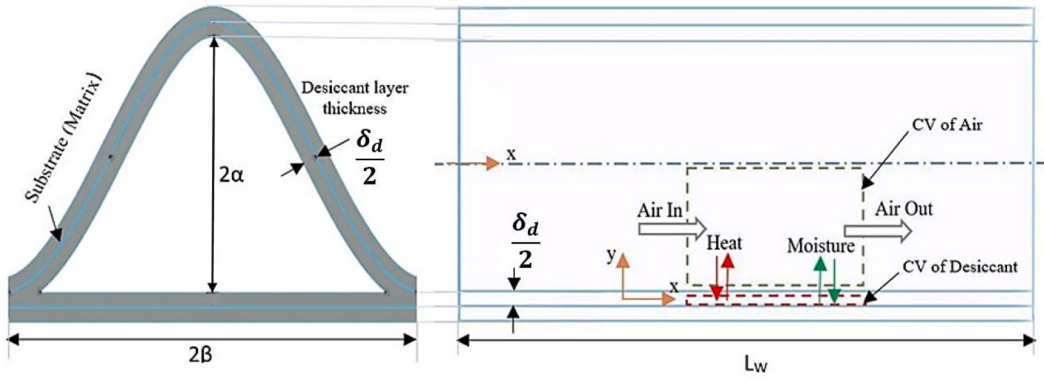


Fig. 3. Front and side view of sinusoidal channel indicating channel geometry and control volume.

3. Mathematical modeling of the proposed system

To develop a mathematical model of the desiccant wheel system, a control volume (CV) of a single sinusoidal channel is selected. The CV is divided into two parts, one for the CV of moist air and the other for the CV of a desiccant layer, as shown in Fig. 3. Mass and energy conservation are applied on each sinusoidal channel CV based on the assumptions below.

3.1. Mathematical model assumptions

The following assumptions have been used to develop a mathematical model.

- One dimensional equation has been assumed for the CV of air.
- The two-dimensional equation has been assumed for the control volume of the desiccant layer because heat conduction and moisture diffusion take place in axial and thickness directions as well as in the desiccant layer, as shown in Fig. 3. The all-sinusoidal channel wall has been considered adiabatic and identical.
- Due to low rotational speed, the centrifugal effect has been neglected.
- The thermophysical property of dry desiccant and dry air and substrate has been assumed to be constant.
- The inlet conditions of moist air are uniform for the flow domain but may vary with time.

Further, some geometric parameters of the channel, like the cross-sectional area of the flow channel (A_{cf}), the cross-sectional area of a desiccant layer (A_{dl}), perimeter (P_{fc}) and hydraulic diameter (D_{hf}) need to be calculated because these will be required for solving the governing equations. These have been expressed in equations (1)–(5).

$$A_{cf} = 2\alpha\beta \quad (1)$$

$$A_{dl} = A_{tc} - A_{cf} \quad (2)$$

Where, A_{tc} represents the total cross-sectional area of one channel which is expressed in equation (3).

$$A_{tc} = \frac{1}{2} (2\alpha + \delta_d)(2\beta + \delta_d) \quad (3)$$

The perimeter of the sinusoidal channel can be expressed as [34]:

$$P_{fc} = 2\beta + 2\sqrt{\beta^2 + (\alpha\pi)^2} \left[\left\{ 3 + \left(\frac{2\beta}{\alpha\pi} \right)^2 \right\} / \left\{ 4 + \left(\frac{2\beta}{\alpha\pi} \right)^2 \right\} \right] \quad (4)$$

The hydraulic diameter of a flow channel is given as [35].

$$D_{hf} = 2\alpha [1.0542 - 0.466(a) - 0.1180(a)^2 + 0.1794(a)^3 - 0.043(a)^4] \quad (5)$$

In equation (5), a is the aspect ratio, and it can be expressed as $a = \frac{2\alpha}{2\beta}$

3.2. Governing equations

Based on the above assumptions, the governing heat and mass transfer equations have been derived. These are expressed below:

Mass conservation equation in the CV of air

$$\rho_{da} A_{cf} \left(u \frac{\partial \omega_a}{\partial x} + \frac{\partial \omega_a}{\partial t} \right) = h_{mc} P_{fc} (\omega_d - \omega_a) \quad (6)$$

Mass conservation equation in the CV of desiccant

$$\begin{aligned} \varepsilon_d A_{dl} \rho_{da} \frac{\partial \omega_d}{\partial t} + \rho_d A_{dl} \Phi \frac{\partial W}{\partial t} &= \rho_d A_{dl} \Phi D_s \left(\frac{\partial^2 W}{\partial x^2} + \frac{\partial^2 W}{\partial y^2} \right) + \\ \varepsilon_d A_{dl} \rho_{da} D_{ko} \left(\frac{\partial^2 \omega_d}{\partial x^2} + \frac{\partial^2 \omega_d}{\partial y^2} \right) + h_{mc} P_{fc} (\omega_a - \omega_d) \end{aligned} \quad (7)$$

Energy conservation equation in the CV of air

$$\rho_{da} (c_{pda} + c_{pv} \omega_a) A_{cf} \left(\frac{\partial T_a}{\partial t} + u \frac{\partial T_a}{\partial x} \right) = h_{hc} P_{fc} (T_d - T_a) - h_{mc} P_{fc} (\omega_d - \omega_a) c_{pv} (T_d - T_a) \quad (8)$$

Energy conservation energy in the CV of desiccant

$$\begin{aligned} \rho_m c_m (1 - \Phi) A_{dl} \frac{\partial T_d}{\partial t} + \rho_d (c_d + W c_{lw}) A_{dl} \Phi \left[\frac{\partial T_d}{\partial t} - \frac{k_d}{\rho_d (c_d + W c_{lw}) \Phi} \left(\frac{\partial^2 T_d}{\partial x^2} + \frac{\partial^2 T_d}{\partial y^2} \right) \right] &= h_{mc} P_{fc} (\omega_a - \omega_d) q_{ad} + h_{hc} P_{fc} (T_a - T_d) \\ + h_{mc} P_{fc} (\omega_d - \omega_a) c_v (T_d - T_a) \end{aligned} \quad (9)$$

In equations (5) to (8), there are five variables (ω_a , ω_d , T_a , T_d and W) but four equations. In order to solve the above equations, some equations will be required which can relate to W and ω_d . First, RH and humidity ratio can be given as:

$$\omega_d = \frac{0.62188 P_v}{P_a - P_v} = \frac{0.62188 R H_d}{P_a / P_{vs} - R H_d} \quad (10)$$

Here, P_{vs} is the saturation pressure vapour, and it can be related using the below relation [35].

$$P_{vs} = e^{23.196 - \frac{3816.44}{T_d - 46.13}} \quad (11)$$

The relation between ω_d and W , is called the equilibrium isotherm equation, and it is expressed as [24]:

$$R H_d = \frac{R \left(\frac{W}{W_{max}} \right)}{1 + (R - 1) \left(\frac{W}{W_{max}} \right)} \quad (12)$$

Where R is the separation factor that determines the nature of isotherms, and it depends on the kind of desiccant material.

In addition, the term diffusion coefficients (D_s and D_{ko}) have been considered in the mass conservation equation of desiccant equation (7). These coefficients can be expressed as:

The surface diffusion coefficient can be expressed as [36].

$$D_s = \frac{D_o}{\tau_g} \exp \left(\frac{-0.974 q_{ad}}{T + 273.15 K} \right) \quad (13)$$

where D_o is the ordinary diffusion coefficient, and it can be expressed as [36].

$$D_o = 1.735 \times 10^{-4} \frac{T_d^{1.685}}{P_{fc}} \quad (14)$$

The term D_{ko} represents the combined diffusivity of ordinary diffusion (D_o) and Knudsen diffusion (D_k), and it can be expressed as below [36].

$$D_{ko} = \frac{1}{\tau_g} \left(\frac{1}{D_o} + \frac{1}{D_k} \right)^{-1} \quad (15)$$

whereas Knudsen diffusion can be expressed as [36].

$$D_k = 97r \left(\frac{T_d}{M} \right)^{0.5} \quad (16)$$

The Nusselt number for the fully developed flow for a single sinusoidal channel is expressed below according to Ref. [36].

$$Nu_{FD} = 1.1791 [1 + 2.7701(a) - 3.9101(a)^2 + 1.997(a)^3 - 0.4966(a)^4] \quad (17)$$

The mass transfer coefficient and Sherwood number (Sh) can be related as:

$$h_{mc} = \frac{\rho_a S h D_{ma}}{D_{hf}} \quad (18)$$

In the above equation, D_{ma} represent the coefficient of mass diffusion vapour in the air which can be expressed as [34]:

Table 2

Input data and experimental conditions used by Kodama [37].

Input data/specifications	Experimental Conditions			
$L_w = 0.2 \text{ m}$	EXP A			
Ratio of Process area to Regeneration area = 3.3	$\omega_{a,in} \& \omega_{r,in} (\text{kg.kg}^{-1})$	$T_{p,in} (\text{K})$	$T_{r,in} (\text{K})$	$u_{p,in} = u_{r,in} (\text{m s}^{-1})$
$2\alpha = 0.0018 \text{ m}$	0.009	298	353	1
$2\beta = 0.0032 \text{ m}$	EXP B			
$\delta_d = 0.0002 \text{ m}$	$\omega_{a,in} \& \omega_{r,in} (\text{kg.kg}^{-1})$	$T_{p,in} (\text{K})$	$T_{r,in} (\text{K})$	$u_{p,in} = u_{r,in} (\text{m s}^{-1})$
	0.00805	298	433	1

$$D_{ma} = 2.302 \times 10^{-5} \frac{P_o}{P} \left(\frac{T}{T_o} \right)^{1.81} \quad (19)$$

$$P_o = 0.98 \times 10^5 \text{ Pa}, T_o = 298 \text{ K}$$

3.3. Boundary and initial conditions

In order to solve the preceding governing equations, boundary conditions will be required. As rotary dehumidifier has been split into four sections. The boundary conditions for each section are given below:

Boundary conditions for temperature and humidity ratio of air

$$T_a(0, t) = T_{p,in} \text{ (Process air)}$$

$$\omega_a(0, t) = \omega_{p,in} \text{ (Process air)}$$

$$T_r(L_w, t) = T_{r,in} \text{ (Regeneration air)}$$

$$\omega_r(L_w, t) = \omega_{r,in} \text{ (Regeneration air)}$$

Boundary conditions for temperature and humidity ratio of desiccant layer

$$\frac{\partial T_d}{\partial x} \Big|_{x=0} = \frac{\partial T_d}{\partial y} \Big|_{y=0} = \frac{\partial T_d}{\partial x} \Big|_{x=L_w=0}$$

$$-k_d \frac{\partial T_d}{\partial y} \Big|_{y=\delta_d/2} = h_{hc} T_d - T_a$$

$$\frac{\partial \omega_d}{\partial x} \Big|_{x=0} = \frac{\partial \omega_d}{\partial y} \Big|_{y=0} = \frac{\partial \omega_d}{\partial x} \Big|_{x=L_w=0}$$

$$\left(-\rho_{da} D_{ka} \frac{\partial \omega_d}{\partial y} - \rho_d D_s \frac{\partial W}{\partial y} \right) \Big|_{y=\delta_d/2} = h_{mc} \omega_d - \omega_a$$

Further, the initial temperature and humidity ratio are assumed to be uniform.

$$T_a(x, 0) = T_{a0}$$

$$T_d(x, 0) = T_d(y, 0) = T_{d0}$$

$$\omega_a(x, 0) = Y_{a0}$$

$$\omega_d(x, 0) = \omega_d(y, 0) = Y_{d0}$$

$$W(x, 0) = W(y, 0) = W_0$$

The above boundary and initial conditions have been applied to solve the governing equations along with auxiliary equations. The partial differential equation (PDE) solver software has been used to obtain the solution of all the above partial differential and algebraic equations. The four programs have been written in the script language of the PDE solver for two processes and two regeneration sections. These programs have been coupled in PDE solver according to the direction of rotation and position of the sections in the desiccant wheel.

3.4. Validation of the developed mathematical model

The developed mathematical model has been validated with the experimental results of Kodama [37] under two experimental

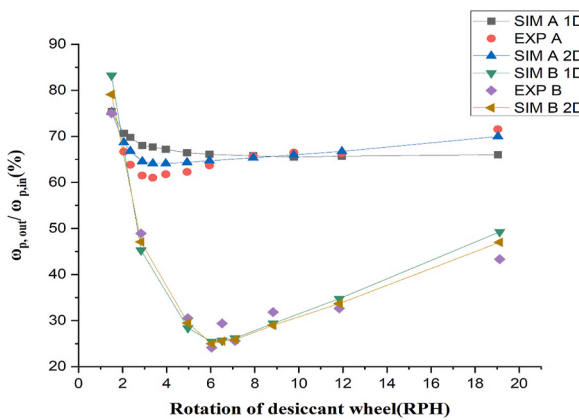


Fig. 4. Validation of model at the specified conditions of Table 2.

Table 3
Angular division of four sectors desiccant wheel for the analysis.

Pair 1 (R2, P1)		Angle (θ) of R1 = 45° and Angle of P2 = 135° is Fixed				
		30	60	90	120	150
	Angle of P1	150	120	90	60	30

Pair 2 (R1, P2)		Angle (θ) of R2 = 105° and Angle of P1 = 75° is Fixed				
		30	60	90	120	150
	Angle of P2	150	120	90	60	30

Table 4
Input data required for the simulation.

Description	Symbol	Fixed value	Variation
Wheel rotational speed	N	15 rph	5-35 rph
Process inlet temperature of P1	TP1	288 K	–
Inlet humidity ratio of P1	ω_{P1}	0.0106 kg. kg ⁻¹	–
The inlet temperature of process air in P2	TP2	303 K	–
Inlet humidity ratio of the wheel (P2, R1, and R2)	ω_{in}	0.0216 kg. kg ⁻¹	–
Regeneration temperature R1 (inlet)	TR1	333 K	318-358 K
Regeneration temperature R2 (inlet)	TR2	318 K	298-318 K
The velocity of process air in P1, P2, R2	u	2 m s ⁻¹	–
The velocity of regeneration air in R1	u	4 m s ⁻¹	–
The height of the channel	2α	18e-4 m	–
The pitch of the channel	2β	32 e-4 m	–
Thickness of the wall	δ _d	2 e-4 m	–
Length of the wheel	L _w	0.2 m	–
Volume ratio	Φ	0.7	–
Heat capacity of matrix or substrate	c _m	880 J kg ⁻¹ . K ⁻¹	–
Desiccant thermal conductivity	k _d	0.22 W m ⁻¹ . K ⁻¹	–
Matrix or substrate density	ρ _m	625 kg. m ⁻³	–
Adsorbent density	ρ _d	790 kg. m ⁻³	–

conditions. The input data and experimental conditions used for the comparison are presented in Table 2.

The same input parameters were taken to validate the mathematical model. Two different humidity ratio (0.009 and 0.00805) of inlet air was taken as experiment A (EXP A) and experiment B (EXP B). In our previous work [24] 1D mathematical model of the desiccant wheel was utilized for investigation. Further, to know the betterment of the 2D model, the 1D model of [24] has also been included in the comparison, as shown in Fig. 4. This shows that trend of the 2D model is like EXP results, and it closely matches the EXP results as compared to the 1D model results. The maximum difference between the 2D Model and EXP results is less than 8%.

4. Results and discussion

The angles of a four-sector desiccant wheel have been clubbed into two pairs for analysis purposes. The process section P1 and the regeneration section R2 are combined in the first pair. Similarly, process section P2 and regeneration section R1 have been combined in the second pair. These pairs have been determined such that, as the desiccant wheel rotates, the P1 section will follow the R2 section,

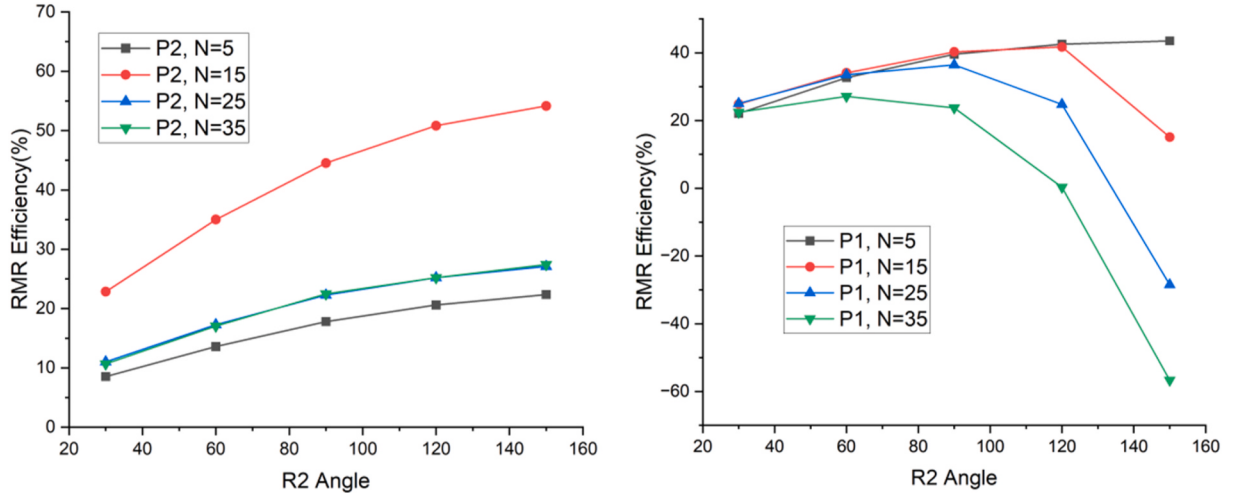


Fig. 5. Variation of RMRE of both process sections (P1 and P2) with the different R2 angles (in degree) at varying rotational speeds from N = 5 to 35 rph.

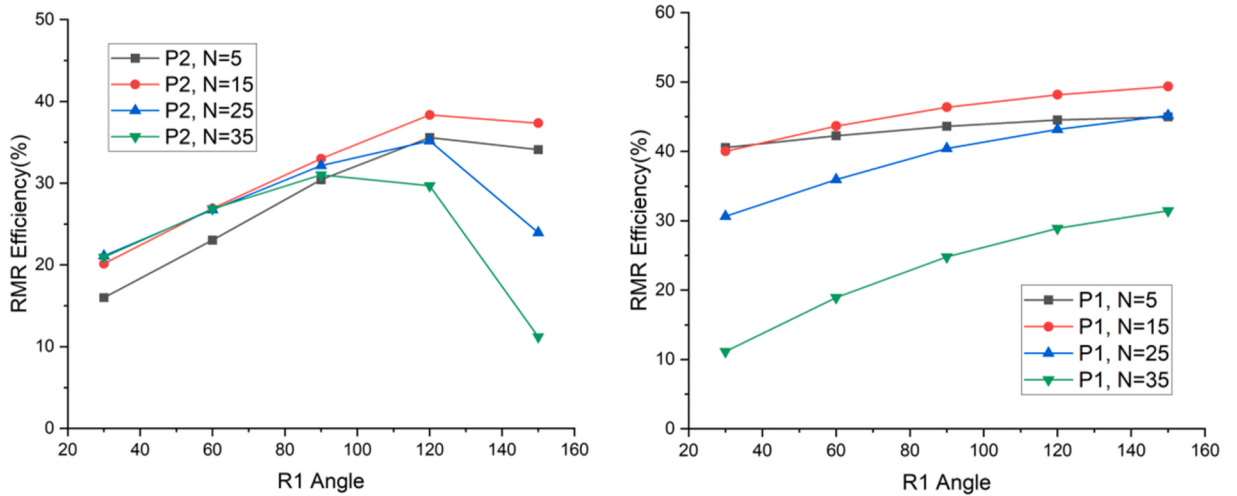


Fig. 6. Variation of RMRE of both process sections (P1 and P2) with the angles (in degree) of R1 at different rotational speeds from N = 5 to 35 rph.

thereby influencing the P1 outflow. Likewise, modifications to the R1 angle and temperature will affect the output of the P2 section. In addition, when the angles of the first pair are altered, the angles of the second pair are fixed, as shown in Table 3.

In this section, the effect of regeneration angles of both the pair (R1 and R2) have been studied at different rotational speeds, regeneration temperatures (T_{R1} and T_{R2}), and P1 inlet temperature. The following performance parameters have been calculated and plotted in the subsequent section for the selection of optimum regeneration angles and operating conditions.

RMRE: The Relative Moisture Removal efficiency (RMRE) represents the ratio of actual and the ideal dehumidification capability of the rotary dehumidifier [38]:

$$RMRE (\%) = \frac{\omega_{in} - \omega_{out}}{\omega_{in}} \times 100 \quad (20)$$

Process exit temperature (T_{P1} and T_{P2}): For this study, the process exit temperature of both P1 and P2 is important as a lower exit temperature is desirable for P1, but a slightly higher exit temperature is desirable for P2. Because P1 has been used for air conditioning while P2 is for dehumidifying, and a slightly higher exit temperature improves the process of dehumidifying.

Dehumidification Coefficient of Performance (DCOP): DCOP of the novel wheel has also been calculated for optimal conditions found in this investigation. The DCOP is the ratio of the heat energy associated with the dehumidified air to the heat energy supplied for regeneration [38]:

$$DCOP = \frac{\dot{m}_p h_{fg} (\omega_{p,in} - \omega_{p,out})}{\dot{m}_r c_p (T_{r,in} - T_{r,out})} \quad (21)$$

Table 5

Optimum regeneration angle at a different rotational speed.

Rotational speed	5 rph	15 rph	25 rph	35 rph
Maximum RMRE of P1 (%)	43.53	41.72	36.40	27.14
Optimum regeneration angle R2	150°	105°	90°	60°
exit Temperature (K) of P1 at optimum R2	296.80	297.02	296.96	296.10
Maximum RMRE of P2 (%)	35.57	38.34	35.17	31.01
Optimum regeneration angle R1	120°	120°	105–120°	105°
Exit Temperature (K) of P2 at optimum R1	319.20 K	318.60 K	318.3 K	316.10 K

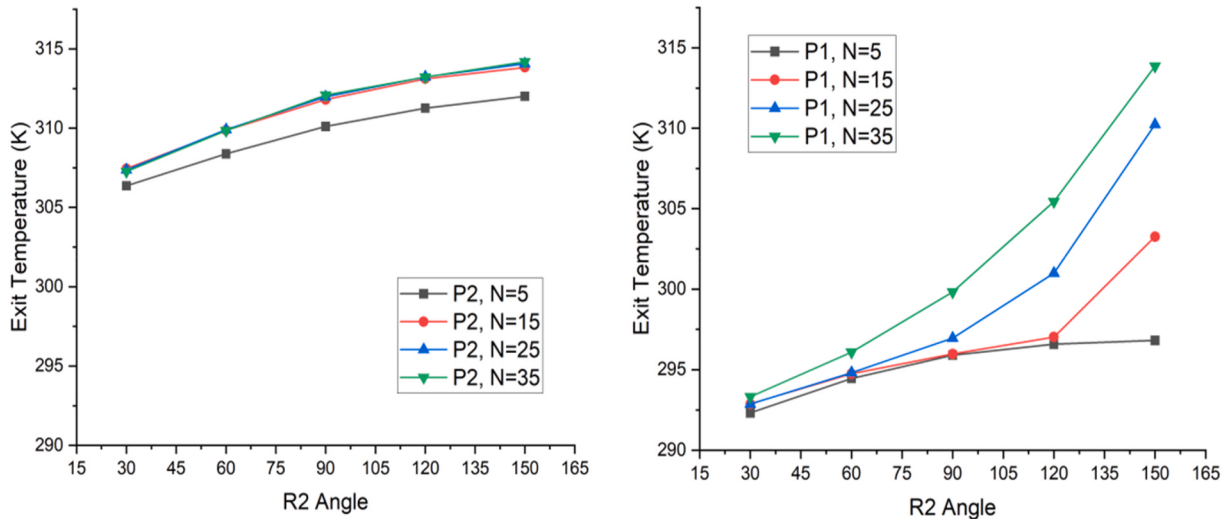


Fig. 7. Variation of exit temperature of both process sections with R2 angles (in degree) at different rotational speeds from N = 5 rph to N = 35 rph.

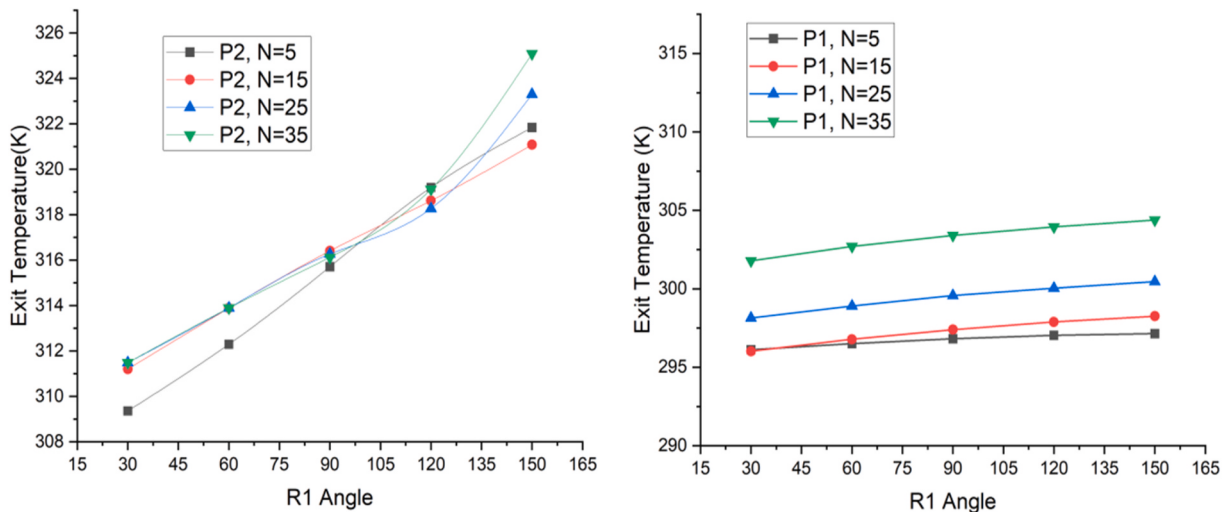


Fig. 8. Variation of exit temperature of both process sections with R1 angles (in degree) at different rotational speeds from N = 5 rph to N = 35 rph.

To simulate the problem and to calculate the performance parameters, the following input data has been used, which are shown in Table 4:

4.1. Effect of regeneration angle (R2 and R1) at the different rotation speeds

From Figs. 5 and 6, it is observed that the effect of the R2 angle is more on the RMRE of P1 as compared to P2. This is due to R2 being the pair of P1 and R1 being the pair of P2. As a result, the R2 angle is determined based on optimizing P1's RMRE and R1 angle based on P2's RMRE. However, increasing the R2 angle also increases the RMRE of P2, which causes rapid and effective regeneration in R1

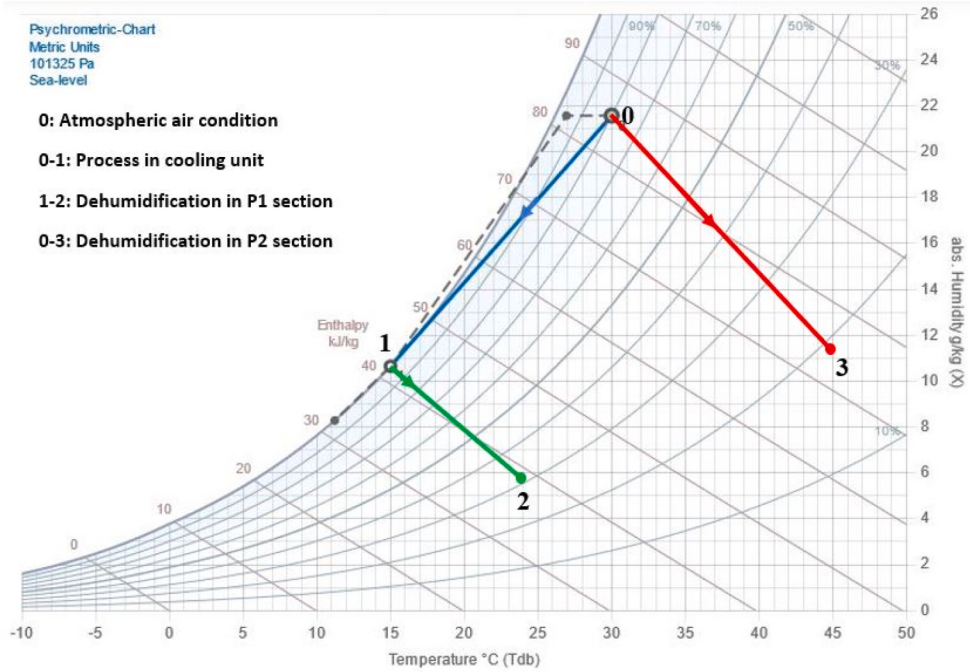


Fig. 9. A psychrometric representation of P1 and P2 streams.

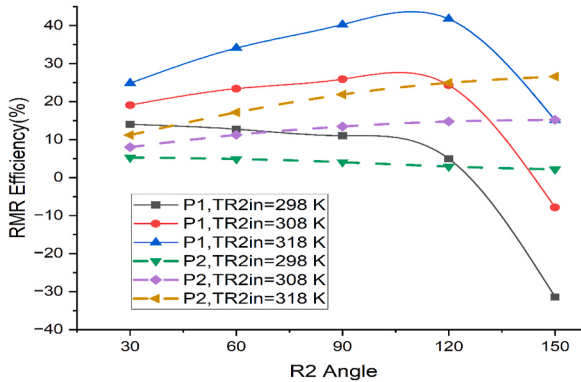


Fig. 10. RMR Efficiency of both process sections at different R2 angles (in degree) and different Regeneration Temperature of R2.

and influences P2. A similar trend has also been obtained when the R1 angle is varied for the second pair. Furthermore, the RMRE of P2 is higher than that of P1 because of the higher regeneration temperature of R1 as compared to R2 and which is desirable for use also.

Fig. 6 shows an optimal rotational speed (15 rph) and regeneration angle ($R2 = 105^\circ$, $R1 = 120^\circ$), at which RMRE is better for both P1 and P2. Too lower and too higher regeneration angles are not desirable for better RMRE. Because too higher regeneration angle decreases the angle of the process section of that pair, and due to this time required for dehumidification in the process section decreases. On the other hand, a too-lower regeneration angle results in poor regeneration performance. However, this performance also depends upon the rotational speed. As depicted in Figs. 5 and 6, the optimum regeneration angle decreases (also shown in Table 5) with an increase in rotational speed because a higher process area is required for increased speed.

It has also been observed that after 105° of R2, RMRE goes down to a negative value in the higher speed ranges (25–35 rph). Because too higher R2 angle causes adsorption in some portion of the R2 section itself, the regeneration temperature has also been kept low. Similarly, too higher speed is not at all desirable for the dehumidification of smaller process sections. The obtained optimum value of regeneration angles is also supported by exit temperatures because at this angle exit temperature of P1 is on the lower side, and beyond this increase in T_e is significant. As the slope of the curve is increasing, and this can be observed in Figs. 7 and 8. Further, the optimum results (exit humidity ratio and temperature) of Figs. 6 and 7 are presented in the psychrometric chart (Fig. 9) along with the cooling coil process for better interpretation.

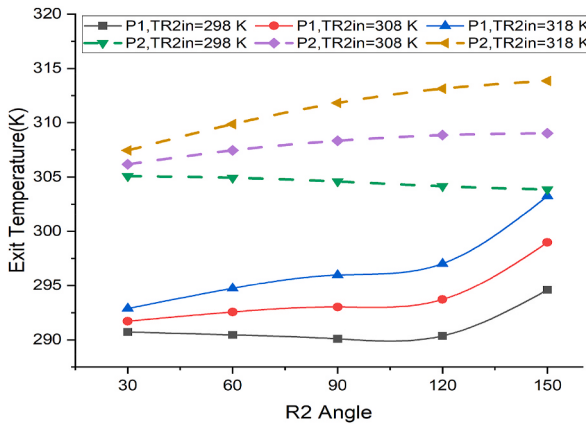


Fig. 11. Exit Temperature of both process sections at different R2 angles (in degree) with the variation of Regeneration Temperature of R2.

Table 6

Optimum regeneration angle (R2) at different regeneration temperatures of R2.

Regeneration Temperature (T_{R2})	298 K	308 K	318 K
Maximum RMRE (%) of P1	14.018	25.90	41.72
Exit temperature of P1 at optimum R2	290.72 K	293.02 K	297.03 K
Optimum regeneration angle R2	30°	90–105°	105–120°

Table 7

Optimum regeneration angle (R1) at different regeneration temperatures of R1.

Regeneration Temperature (T_{R1})	318 K	338 K	358 K
Optimum regeneration angle R1	120°	120°	120°
RMRE % of P2 at optimum R1	24.12	41.32	57.01
Exit temperature of P2 at optimum R1	312.78 K	320.66 K	329.02 K

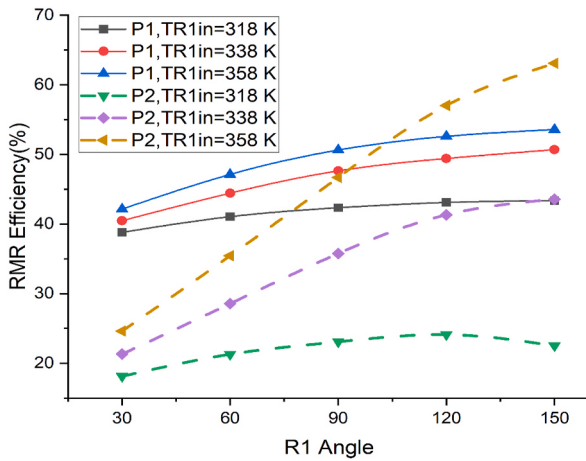


Fig. 12. RMR Efficiency of both process sections at different R1 angles (in degree) and different Regeneration Temperature of R1.

4.2. Effect of regeneration angle (R2) at different regeneration temperatures of R2

In this case (Figs. 10 and 11) also, the trend of RMRE and exit temperature are like to the previous cases. But here, regeneration temperature varied on the lower side. At very low regeneration temperatures (298–398 K), RMRE goes down to a negative value beyond 120° R2. So, when the room return air of lesser regeneration temperature of the air is used for regeneration, in that case, the regeneration should be lower than 120°. However, at 318 K, the RMRE is positive at any angle of regeneration angle and better than the other cases. The optimum value of the regeneration angle at different regeneration temperatures is presented in Table 6 (R2 angle) and

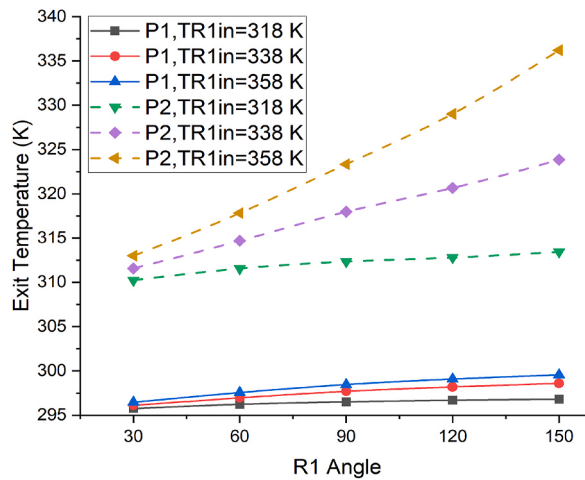


Fig. 13. Exit Temperature of both process sections at different R1 angles (in degrees) with the variation of Regeneration Temperature of R1.

Table 7 (R1 angle).

4.3. Effect of regeneration angle (R1) at different regeneration temperatures of R1

Figs. 12 and 13 shows that the slope of the graph increases as the regeneration temperature rises because proper regeneration is achieved at higher temperatures. In contrast, as the R1 angle increases, RMRE and exit temperature increase, but the curve starts flattening after 120°. Further, a higher angle of R1 results in higher carryover heat in P1, which is visible in Fig. 13.

Finally, from the analysis of the above cases, the obtained value of optimum regeneration angles for R2 and R1 are 100–110° and 115–125°, respectively. Similarly, at these conditions, the obtained value of the Dehumidification Coefficient of Performance (DCOP) from equation (21) is 0.53.

5. Conclusions

In this work, a novel configuration of four sector desiccant wheels for different dehumidifying conditions; has been mathematically investigated. To calculate the RMRE and exit temperature of both process sections, the regeneration angle has been varied at various rotational speeds and regeneration temperatures. The following conclusions have been drawn from the results of this study:

1. The optimal rotational speed of the wheel obtained is 15 rph at optimum regeneration angles of R2 and R1 are 100–110° and 115–125°, respectively. Further, the reduced optimum regeneration angle is reported with increased rotational speeds.
2. The maximum RMRE of P2 reaches 57% at 120° R1 indicating its potential use for dehumidifying applications.
3. The exit temperature obtained from P1 ranges from 290 K to 298 K at 15 rph when inlet temperature P1 is fixed at 288 K, indicating its potential use for cooling applications.

Because of the four sectors, we can choose the different regeneration temperatures in R1 and R2. Similarly, we can maintain different inlet conditions in P1 and P2 to get different output conditions, as a cooling coil is introduced in the P1 section of this study. But this feature is not available in two-sector wheels. Since we are maintaining a lower temperature (but sacrificing the RMRE of P1) in R2 (318 K) and the position of R1 (in between P1 and P2) is such, it reduces the carryover heat. Due to this, the exit temperature obtained from P1 is significantly lower than P2. Therefore, the optimal angular division for the analyzed four-sector wheel is determined as R2 = 105°, P1 = 75°, R1 = 120°, and P2 = 60° for two different applications (dehumidification and HVAC). For this optimal design configuration, the DCOP of the system is computed as 0.53 at the wheel rotation speed of 15 rph.

Author statement

Ashutosh Kumar Verma: Conceptualization, Manuscript writing, Result determination, Software and validation of result.

Laxmikant Yadav: Conceptualization, Methodology, Visualization, Manuscript Writing, Formal analysis, Supervision.

Declaration of competing interest

The authors declare that they have no known competing financial interests or personal relationships that could have appeared to influence the work reported in this paper.

Data availability

The data that has been used is confidential.

References

- [1] K.N. Cerci, E. Hurdogan, Performance assessment of a heat pump assisted rotary desiccant dryer for low temperature peanut drying, *Biosyst. Eng.* 223 (2022) 1–17, <https://doi.org/10.1016/j.biosystemseng.2022.08.009>.
- [2] Y.E. Guzelel, U. Olmus, O. Buyukalaca, Simulation of a desiccant air-conditioning system integrated with dew-point indirect evaporative cooler for a school building, *Appl. Therm. Eng.* 217 (2022), 119233, <https://doi.org/10.1016/j.applthermaleng.2022.119233>.
- [3] S.P. Denyer, R.M. Baird, *Guide to Microbiological Control in Pharmaceuticals and Medical Devices*, second ed., CRC Press, Boca Raton, 2006.
- [4] J. Zhao, Z. Lu, N. Liu, H.-W. Lee, M.T. McDowell, Y. Cui, Dry-air-stable lithium silicide-lithium oxide core-shell nanoparticles as high-capacity pre lithiation reagents, *Nat. Commun.* 5 (2014) 5088, <https://doi.org/10.1038/ncomms6088>.
- [5] D. Okposio, *Net Zero Desiccant Assisted Evaporative Cooling for Data Centers* (Doctoral Dissertation, Purdue University Graduate School, 2020).
- [6] American Society of Heating, Refrigerating and Air-Conditioning Engineers. "Energy Recovery Ventilators and Ventilation Energy Recovery.", ASHRAE Handbook - HVAC Systems and Equipment, 2017.
- [7] D. Jani, M. Mishra, P.K. Sahoo, Experimental investigation on solid desiccant-vapor compression hybrid air-conditioning system in hot and humid weather, *Appl. Therm. Eng.* 104 (2016) 556–564, <https://doi.org/10.1016/j.applthermaleng.2016.05.104>.
- [8] D. Jani, M. Mishra, P.K. Sahoo, Solid desiccant air conditioning - a state of the art review, *Renew. Sustain. Energy Rev.* 60 (2016) 1451–1469, <https://doi.org/10.1016/j.rser.2016.03.031>, 2016.
- [9] C.K. Qin, G. Schmitz, *Engine-driven desiccant-assisted hybrid air-conditioning system*, in: *23rd World Gas Conference 15, 2006. Amsterdam*.
- [10] U. Olmuş, Y.E. Güzelel, E. Pınar, A. Özbeş, O. Büyükalaca, Performance assessment of a desiccant air-conditioning system combined with dew-point indirect evaporative cooler and PV/T, *Sol. Energy* 231 (2022) 566–577, <https://doi.org/10.1016/j.solener.2021.12.004>.
- [11] M.M. Abd-Elhady, M.S. Salem, A.M. Hamad, I.I. Sharkawy, Solid desiccant-based dehumidification systems: a critical review on configurations, techniques, and current trends, *Int. J. Refrig.* 133 (2022) 337–352, <https://doi.org/10.1016/j.ijrefrig.2021.09.028>.
- [12] K. Nagaya, Y. Li, Z. Jin, M. Fukumuro, Y. Ando, A. Akaishi, Low-temperature desiccant-based food drying system with airflow and temperature control, *J. Food Eng.* 75 (2006) 71–77, <https://doi.org/10.1016/j.jfoodeng.2005.03.051>.
- [13] M.N. Golubovic, H.M. Hettiarachchi, W.M. Worek, Evaluation of rotary dehumidifier performance with and without heated purge, *Int. Commun. Heat Mass Tran.* 34 (2007) 785–795, <https://doi.org/10.1016/j.icheatmasstransfer.2007.03.011>.
- [14] A. Yadav, V.K. Bajpai, Analysis of various designs of a desiccant wheel for improving the performance using a mathematical model, *J. Renew. Sustain. Energy* 5 (2) (2013), <https://doi.org/10.1063/1.4794748>, 10.1063/1.4794748.
- [15] A. Yadav, Analysis of desiccant wheel with purge sector for improving the performance using a mathematical model, *Int. J. Air Cond. Refrig.* 22 (1) (2014), 1450004, <https://doi.org/10.1142/S2010132514500047>.
- [16] L. Yadav, A. Yadav, Mathematical investigation of purge sector angle for clockwise and anticlockwise rotation of desiccant wheel, *Appl. Therm. Eng.* 93 (2016) 839–848, <https://doi.org/10.1016/j.applthermaleng.2015.10.062>.
- [17] M.A. Mandegari, S. Farzad, G. Angrisani, H. Pahlavanzadeh, Study of purge angle effects on the desiccant wheel performance, *Energy Convers. Manag.* 137 (2017) 12–20, <https://doi.org/10.1016/j.enconman.2017.01.042>.
- [18] S. Motaghian, H. Pasdarshahri, Regeneration energy analysis and optimization in desiccant wheels using purge mechanism, *J. Build. Eng.* 27 (2020), 100980, <https://doi.org/10.1016/j.jobe.2019.100980>.
- [19] A. Yadav, L. Yadav, Comparative performance of desiccant wheel with effective and ordinary regeneration sector using mathematical model, *Heat Mass Tran.* 50 (2014) 1465–1478, <https://doi.org/10.1007/s00231-014-1349-6>.
- [20] A. Yadav, L. Yadav, Comparative performance of different sector arrangement in a desiccant wheel using a mathematical model, *Heat Tran. Asian Res.* 44 (2) (2015) 133–153, <https://doi.org/10.1002/htrj.21103>.
- [21] L. Yadav, A. Yadav, Effect of different arrangements of sector on the performance of desiccant wheel, *Heat Mass Tran.* 54 (2018) 7–23, <https://doi.org/10.1007/s00231-017-2092-6>.
- [22] A.K. Prasad, L. Yadav, A. Yadav, Comparative analysis of different design of rotary dehumidifier, *Heat Tran. Asian Res.* 54 (Issue 6) (2018) 2193–2215, <https://doi.org/10.1002/htrj.21480>.
- [23] A.M. Elzahby, A.E. Kabeel, M.M. Bassuoni, M. Abdelaied, A mathematical model for predicting the performance of the solar energy assisted hybrid air conditioning system, with one-rotor six-stage rotary desiccant cooling system, *Energy Convers. Manag.* 77 (2014) 129–142, <https://doi.org/10.1016/j.enconman.2013.08.052>.
- [24] A.K. Verma, L. Yadav, D. Agrawal, A. Dhamija, G. Rajneesh Bijalwan, Mathematical investigation of two-stage dehumidification from single rotary dehumidifier with and without precooling, *Numer. Heat Tran., Part A: Applications* 82 (3) (2022) 82–108, <https://doi.org/10.1080/10407782.2022.2066922>.
- [25] L. Yadav, A. Yadav, Parametric analysis of desiccant wheel for air conditioning application, *Heat Tran. Asian Res.* 47 (6) (2018) 771–793, <https://doi.org/10.1002/htrj.21338>.
- [26] A. Kodama, N. Watanabe, T. Hirose, M. Goto, H. Okano, Performance of a multipass honeycomb adsorber regenerated by a direct hot water heating, *Adsorption* 11 (2005) 603–608.
- [27] R. Narayanan, W.Y. Saman, S.D. White, A non-adiabatic desiccant wheel: modeling and experimental validation, *Appl. Therm. Eng.* 61 (2) (2013) 178–185, <https://doi.org/10.1016/j.applthermaleng.2013.07.007>.
- [28] M.J. Goldsworthy, S. White, Design and performance of an internal heat exchange desiccant wheel, *Int. J. Refrig.* 39 (2014) 152–159, <https://doi.org/10.1016/j.ijrefrig.2013.10.009>.
- [29] X. Zhou, M. Goldsworthy, A. Sproul, Performance investigation of an internally cooled desiccant wheel, *Appl. Energy* 224 (2018) 382–397, <https://doi.org/10.1016/j.apenergy.2018.05.011>.
- [30] Y.E. Guzelel, U. Olmus, K.N. Cerci, O. Buyukalaca, New multiple regression and machine learning models of rotary desiccant wheel for unbalanced flow conditions, *Int. Commun. Heat Mass Tran.* 134 (2022), 106006, <https://doi.org/10.1016/j.icheatmasstransfer.2022.106006>.
- [31] Y.E. Guzelel, U. Olmus, K.N. Cerci, O. Buyukalaca, Comprehensive modeling of rotary desiccant wheel with different multiple regression and machine learning methods for balanced flow, *Appl. Therm. Eng.* 199 (2021), 117544, <https://doi.org/10.1016/j.applthermaleng.2021.117544>.
- [32] J. Jeong, S. Yamaguchi, K. Saito, S. Kawai, Performance analysis of four-partition desiccant wheel and hybrid dehumidification air-conditioning system, *Int. J. Refrig.* 33 (3) (2010) 496–509, <https://doi.org/10.1016/j.ijrefrig.2009.12.001>.
- [33] Web 3: American Society of Heating, Refrigerating and Air-Conditioning Engineers [Online], Available: https://www.ashrae.org/file%20library/technical%20resources/covid-19/i-p_a19_ch09_health_care_facilities.pdf.
- [34] X.J. Zhang, Y.J. Dai, R.Z. Wang, A simulation study of heat and mass transfer in a honeycombed rotary desiccant dehumidifier, *Appl. Therm. Eng.* 23 (8) (2003) 989–1003, [https://doi.org/10.1016/S1359-4311\(03\)00047-4](https://doi.org/10.1016/S1359-4311(03)00047-4).
- [35] R. Narayanan, W.Y. Saman, S.D. White, M. Goldsworthy, Comparative study of different desiccant wheel designs, *Appl. Therm. Eng.* 31 (2011) 1613–1620, <https://doi.org/10.1016/j.applthermaleng.2011.01.043>.
- [36] L.Z. Zhang, J.L. Niu, Performance comparisons of desiccant wheels for air dehumidification and enthalpy recovery, *Appl. Therm. Eng.* 22 (2003) 1347–1367, [https://doi.org/10.1016/S1359-4311\(02\)00050-9](https://doi.org/10.1016/S1359-4311(02)00050-9), 2002.
- [37] A. Kodama, *Experimental Study on Optimization of a Honeycomb Rotor Continuous Adsorber Operated with Thermal Swing*, Ph.D. Dissertation, Kumamoto University Japan, Feb., 1995.
- [38] T.S. Ge, F. Ziegler, R.Z. Wang, A mathematical model for predicting the performance compound desiccant wheel (a model of compound desiccant wheel), *Appl. Therm. Eng.* 30 (2010) 1005–1015, <https://doi.org/10.1016/j.applthermaleng.2010.01.012>.